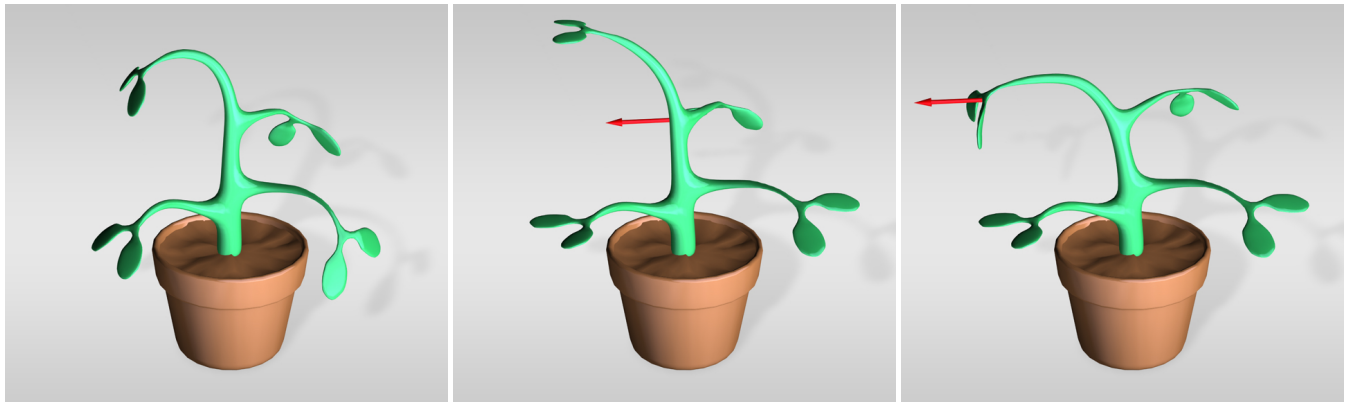


# Reformulating Hyperelastic Materials with Peridynamic Modeling

Liyou Xu<sup>1</sup>, Xiaowei He<sup>†2</sup>, Wei Chen<sup>1</sup>, Sheng Li <sup>‡1</sup> and Guoping Wang<sup>1</sup>

<sup>1</sup>Peking University, <sup>2</sup>State Key Lab. of CS, ISCAS



**Figure 1:** The flower example. We simulate the flower as a nonlinear and heterogeneous material where the material stiffness of the stem is larger than that of the leaves. (a) Imposed with a gravity; (b) Imposed with an external force on the stem; (c) Imposed with an external force on a leaf.

## Abstract

Peridynamics is a formulation of the classical elastic theory that is targeted at simulating deformable objects with discontinuities, especially fractures. Till now, there are few studies that have been focused on how to model general hyperelastic materials with peridynamics. In this paper, we target at proposing a general strain energy function of hyperelastic materials for peridynamics. To get an intuitive model that can be easily controlled, we formulate the strain energy density function as a function parameterized by the dilatation and bond stretches, which can be decomposed into multiple one-dimensional functions independently. To account for nonlinear material behaviors, we also propose a set of nonlinear basis functions to help design a nonlinear strain energy function more easily. For an anisotropic material, we additionally introduce an anisotropic kernel to control the elastic behavior for each bond independently. Experiments show that our model is flexible enough to redapproximately regenerate various hyperelastic materials in classical elastic theory, including St.Venant-Kirchhoff and Neo-Hookean materials.

## CCS Concepts

•Computer Graphics → Three-Dimensional Graphics-Animation;

## 1. Introduction

Since peridynamics was originally proposed by Silling [Sil00] with the ambition to uniformly solve problems involving both continuities and discontinuities, it has been mainly applied by

researchers in engineering to study crack formation and propagation [SB05, GSS07, HHBS12]. Although redperidynamics can naturally handle crack surfaces the same way as interior regions due to the integration nature, the theoretical equivalence of peridynamics in modeling continuous regions compared to continuum mechanics remains unclear. Till now, only some specific model in peridynamics has been proven to redconverge to the redclassical elastic theory [SL08], which means a lot of mature theories and experi-

<sup>†</sup> xiaowei@iscas.ac.cn.

<sup>‡</sup> lisheng@pku.edu.cn.

ences in continuum mechanics cannot be directly applied to peridynamics. This also explains why most of the work in peridynamics only consider simple elastic models, e.g., a purely bond-base model [LBC<sup>\*</sup>14] or a simple linear elastic model [HWW17]. So far, how to extend peridynamics to model general hyperelastic materials still remains a redchallenging problem.

In computer graphics, simulation of complex three-dimensional redhyperelastic materials has been mostly carried out with a finite element method (FEM), which could involve nonlinearity [BJ05, STC<sup>\*</sup>12, XSZB15], anisotropy [BC00, LB14, LB15] or both [PDA01, BBO<sup>\*</sup>09, KMOD09]. Most of these studies are based on empirical constitutive models. Therefore, to get a desired simulation result, it usually requires to choose a specific constitutive model as well as do some tuning of the physical parameters. However, in certain cases, we even do not know which constitutive model is the right one to choose, due to the complexity of real-world materials. Besides, the simulation results of numerical methods also depend on many factors, such as the time step, the mesh size and the numerical solver, etc. Usually, it is not an easy task to remove all these influences.

To address above difficulties, Xu and colleagues [XSZB15] proposed to decompose the strain energy density function into several one-dimensional scalar functions, parameterized by the principal stretches of the deformation gradient. Then, by editing each scalar function separately using piecewise splines, their method can effectively regenerate various hyperelastic materials. However, since there is no equivalent formulation of the proposed strain energy function for peridynamics, it is not an easy task to directly apply their method for modeling hyperelastic materials within peridynamics. Recently, He and colleagues [HWW17] demonstrated that the strain energy density function of a linear elastic material in continuum mechanics can be reformulated as reda collection of the strain energy stored independently on each bond. Unfortunately, their elastic model cannot be extended to hyperelastic materials.

In this paper, we aim at reformulating the strain energy function of hyperelastic materials in continuum theory for peridynamics, motivated by [XSZB15]. Instead of representing the strain energy as a function of the principal stretches, we formulate it as a combination of separate one-dimensional functions which are parameterized by the dilatation and the bond stretches. To account for nonlinear material behaviors, we propose a set of nonlinear basis functions to help design a nonlinear strain energy function easily and intuitively. The separation of strain energies also greatly facilitates the generation of anisotropic materials, which can redbe realized by integrating an anisotropic kernel function. Experiments show that our model is flexible enough to redapproximately regenerate several hyperelastic materials in classical elastic theory, e.g., St.Venant-Kirchhoff or Neo-Hookean materials.

To summarize, our contributions are as follows:

- A reformulated strain energy density function of hyperelastic materials for peridynamics, parameterized by the dilatation and bond stretches.
- A set of one-dimensional basis functions satisfying three necessary conditions, ensuring plausible hyperelastic material design.
- A simple technique to control the material anisotropy.

## 2. Related Work

In computer graphics, FEM is the most commonly used method to simulate deformable objects. Early works have been mainly focused on simple linear elastic models [GM97], which is only suitable for small deformations. O'Brien and Hodgins [OH99] used FEM for the modeling of brittle fracture. Müller and Gross [MG04] presented a linear corotational FEM to model large deformations. McAdams and colleagues later [Mzs<sup>\*</sup>11] redextended the corotational FEM for the simulation of skeleton driven, high resolution elasticity models. Civit-Flores and colleagues also redapplied the corotational FEM to simulate large deformations by redaddressing the element collapse and inversion problem. However, the linear elastic model is usually too simple to cover all real-world materials. To model nonlinear elastic materials, Wu and colleagues [WDGT01] proposed nonlinear FEM using mass lumping to produce a diagonal mass matrix that allows real time computation. Volino and colleagues [VMTF09] took the material nonlinearity into consideration for accurate cloth simulation. Xu and colleagues [XSZB15] proposed a more general nonlinear FEM model that allows easier design of isotropic nonlinear materials. Li and Barbić investigated both linear anisotropic materials as well as general linear (non-orthotropic) anisotropic materials in [LB15]. Others also have considered material heterogeneity in material modeling [KMOD09, CLSM15].

Elastic objects have also been widely modeled with meshless methods. One popular approach is the smoothed particle hydrodynamics (SPH) method, which was initially invented for astrophysical problems. Researchers in computer graphics later extended SPH to animate elastic bodies by Desbrun and Gascuel [DG96]. To animate large deformations, Becker and colleagues [BIT09] presented a co-rotational SPH formulation for elastic bodies. Jones and collaborators [JWJ<sup>\*</sup>14] directly embedded the deformation gradient to animate elastoplastic material. Alternately, other researchers have directly use constraints instead of elastic forces to simulate deformable objects [MHHR07, RJ07, GHF<sup>\*</sup>07]. Müller and Chentanez [MC11] used oriented particle stored with rotation and spin to simulate various types of solids, including rigid, plastic and soft bodies. Liu and colleagues [LBOK13] propose a solver based on block coordinate descent to animate cloth in real time. Macklin and colleagues [MMCK14] later build a unified GPU-based system to model various materials. Since PBD has the drawbak that the simulation accuracy is affected by the iteration number, Bouaziz and collaborators [BML<sup>\*</sup>14] developed a fast and robust projective dynamics simulator by including geometric constraints as strain energies in a quadratic form. Wang and Yang [WY16] proposed a new gradient descent method using Jacobi preconditioning and Chebyshev acceleration to solve nonlinear elastic objects on GPU. Liu and colleagues [LBK17] showed that Projective Dynamics can be interpreted as a quasi-Newton method, therefore proposed a fast method to simulate various hyperelastic materials. Rahul and colleagues [NOB16] proposed an ADMM method which extends the Projective Dynamics and is applicable to a broad range of objective functions including nonlinear models and hard constraints.

As we know, the governing equations in continuum mechanics are usually in differential form. They are not quite suitable for complex elastic materials involving discontinuities. Therefore,

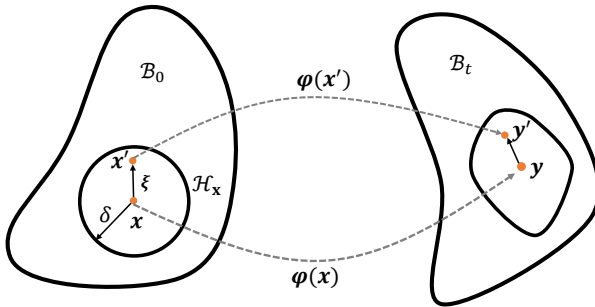


**Figure 2:** Schematic representation of a peridynamic body.

Silling [Sil00] proposed peridynamics to uniformly handle continuous and discontinuous materials. Since its essence is to use integration to compute the force on a material particle, it can be easily integrated into a neural network to develop new material models. The capability of original peridynamics model based on bond is rather limited. It even cannot model materials with different Poisson's ratios. Silling and colleagues [SEW\*07] generalized the bond-based peridynamics to a state-based model, thus allow for modeling of elastic material with different Poisson's ratios. Levine and colleagues [LBC\*14] revisited the spring-mass systems to the animation of brittle fracture from a peridynamic perspective. Chen and colleagues [CZZ\*17] applied peridynamics to simulate a wide range of material phenomena including elasticity, plasticity, and fracture. To improve the simulation performance, He and colleagues [HWW17] proposed a projective method motivated by the position-based method. Their method is robust and efficient to model versatile elastoplastic materials. However, the simulation accuracy remains unverified. Besides, how to accurately regenerate any elastic behaviors with peridynamics is also not clear.

### 3. Background and Motivation

For completeness, we briefly review the state-based peridynamic theory and introduce some basic notations that will be used in the following context. Let  $\mathcal{B}_0 \subset \mathbb{R}^n$  be the reference configuration of a deformable body at time  $t_0$  and  $\mathcal{B}_t \subset \mathbb{R}^n$  be the transformed configuration at time  $t$ . Under the deformation mapping  $\varphi : \mathcal{B}_0 \rightarrow \mathcal{B}_t$ , points  $\mathbf{x}$  and  $\mathbf{x}'$  are mapped to  $\mathbf{y}$  and  $\mathbf{y}'$  respectively. A bond for point  $\mathbf{x}$  is defined as

$$\xi = \mathbf{x}' - \mathbf{x}, \quad (1)$$

with  $\mathbf{x}'$  representing a point in the neighborhood of point  $\mathbf{x}$  which is typically defined as follows

$$\mathcal{H}_{\mathbf{x}} = \{\xi \in \mathcal{B}_0 | \mathbf{x} + \xi \in \mathcal{B}_0, \|\xi\| < \delta\}, \quad (2)$$

where  $\delta$  is the horizon radius. If not specified, we typically set the horizon radius to be two times of the particle sampling distance  $d$ . A schematic illustration of a peridynamic body is show in Figure 2.

Let  $\mathcal{L}_m$  denote the set of all tensors of order  $m$ , a state of order  $m$  in state-based peridynamics is defined as a mapping function from a bond  $\xi$  to a tensor of order  $m$  as follows

$$A(\xi) : \mathcal{H} \rightarrow \mathcal{L}_m \quad (3)$$

where the bracket notation is used merely to distinguish a state from the mapping function between  $\mathcal{B}_0$  and  $\mathcal{B}_t$ . What distinguishes peridynamics from classical continuum mechanics is that the theory is inherently non-local that material points are assumed to interact through long-range forces represented as a force vector-state  $\mathbf{T}(\xi)$ . Therefore, the governing equations of motion in peridynamics can be formulated as

$$\rho \ddot{\mathbf{u}} = \int_{\mathcal{H}_{\mathbf{x}}} \left\{ \mathbf{T}(\xi) - \mathbf{T}'(-\xi) \right\} dV_{\xi} + \mathbf{b}, \quad (4)$$

in which  $\rho$  is the density,  $\mathbf{u} = \mathbf{y} - \mathbf{x}$  is the displacement field,  $\mathbf{T}$  is a pairwise force whose value is the force vector that point  $\mathbf{x}$  exerts on point  $\mathbf{x}'$ ,  $\mathbf{b}$  is the body force per volume. Note that we have neglected the dependence on  $\mathbf{x}$  and  $t$  for the sake of brevity, e.g.,  $\rho$  is an abbreviation for  $\rho(\mathbf{x}, t)$ ,  $\mathbf{T}(\xi) \equiv \mathbf{T}[\mathbf{x}, t](\xi)$  and  $\mathbf{T}'(\xi) \equiv \mathbf{T}[\mathbf{x}', t](\xi)$ .

Consider an arbitrary deformation vector state  $\mathbf{Y}(\xi) \equiv \mathbf{y}' - \mathbf{y}$ , the general form of an elastic constitutive model in state-based peridynamics is written as

$$\mathbf{T} = \hat{\mathbf{T}}(\mathbf{Y}) \quad (5)$$

by neglecting all variables other than the current deformation vector state. It means the value of  $\mathbf{T}(\xi)$  may depend on all local bonds in  $\mathcal{H}_{\mathbf{x}}$ . Since  $\mathcal{H}_{\mathbf{x}}$  contains an infinite number of bonds, the constitutive relationship in Equation 5 is therefore too complex for practical implementation. As we know, the constitutive equation in continuum mechanics describes a relationship between a strain tensor and a stress tensor, both of which contain 6 independent values for an arbitrary deformation in three-dimensional space. That is to say, a bunch of relationships in Equation 5 are redundant for modeling real-world materials. However, it is also an oversimplification to assume that any pair of particles interact only through the current bond and are totally independent of all other neighboring bonds, as was done in the bond-based peridynamics [Sil00]. This motivates us to propose a new constitutive model for hyperelastic materials by combining bond-based forces and state-based forces together. The purpose is to guarantee the proposed constitutive equation is easy for code implementation, but can model a variety of nonlinear and anisotropic materials.

Before deriving a general constitutive model for hyperelastic materials, we first investigate the linear peridynamic solid proposed by Silling and his colleagues [SEW\*07]

$$W = \frac{k(\theta - 3)^2}{2} + \frac{\alpha}{2} \int_{\mathcal{H}_{\mathbf{x}}} w(\xi) \left( e(\xi) - \frac{\theta - 3}{3} x(\xi) \right)^2 dV_{\xi} \quad (6)$$

where  $k$  is the bulk module,  $\alpha$  equals  $\frac{15\mu}{m}$  with  $\mu$  representing the shear module and  $m = \int_{\mathcal{H}_{\mathbf{x}}} w(\xi) x(\xi) x(\xi) dV_{\xi}$ ,  $w(\xi)$  is a weighting function,  $e(\xi)$  represents the extension scalar state defined as

$$e(\xi) = y(\xi) - x(\xi) \quad (7)$$

with  $y(\xi) = \|\mathbf{y}' - \mathbf{y}\|$ ,  $x(\xi) = \|\mathbf{x}' - \mathbf{x}\|$  and  $\theta$  represents the dilatation calculated from the following formula

$$\theta = \frac{3 \int_{\mathcal{H}_{\mathbf{x}}} w(\xi) x(\xi) y(\xi) dV_{\xi}}{\int_{\mathcal{H}_{\mathbf{x}}} w(\xi) x(\xi) x(\xi) dV_{\xi}} \quad (8)$$

For a small deformation, the physical meaning of  $\theta$  is similar to the first invariant of the deformation gradient tensor  $\mathbf{F}$  in continuum

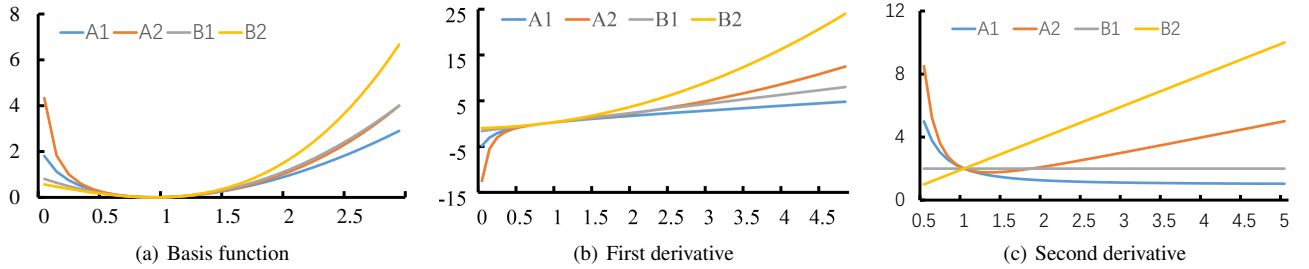


Figure 3: redIllustration of the basis functions.

mechanics. To see this, considering an isotropic deformation with the form  $y(\xi) = (1 + \varepsilon_0)x\langle\xi\rangle$  where  $\varepsilon_0$  is a small constant, i.e.,  $\varepsilon_0 \ll 1$ , we have the following relationship

$$\theta = 3(1 + \varepsilon_0) = \lambda_1 + \lambda_2 + \lambda_3, \quad (9)$$

where  $\lambda_i$  are the principal stretches of the deformation gradient  $\mathbf{F}$ . By invoking the definition of  $\theta$  and doing some simple algebraic operations, Equation 6 can be reformulated as a function of the dilatation  $\theta$  and bond stretches  $\tau\langle\xi\rangle = y\langle\xi\rangle/x\langle\xi\rangle$  as follows

$$W(\theta, \tau\langle\xi\rangle) = \underbrace{\left(\frac{k}{2} - \frac{\alpha m}{18}\right)(\theta - 3)^2}_{g(\theta)} + \underbrace{\frac{\alpha}{2} \int_{\mathcal{H}_x} w\langle\xi\rangle (\tau\langle\xi\rangle - 1)^2 (x\langle\xi\rangle)^2 dV_\xi}_{h(\tau\langle\xi\rangle)}. \quad (10)$$

From the above definition, it can be noted that the strain energy actually consists of two independent parts, the first part is a function of  $\theta$  while the second part is a function of  $\tau\langle\xi\rangle$ . The advantage of separating  $\text{red}\theta$  and  $\tau\langle\xi\rangle$  is significant, we can reduce the deformation space and control each part independently, thus redmaking the designing of a new hyperelastic material easier and more intuitive, as was done in [XSZB15]. Although both  $\text{red}g(\theta)$  and  $h(\tau\langle\xi\rangle)$  should be in a quadratic form for the linear elastic solid, the strain energy density function in Equation 10 can be easily extended to model more complex hyperelastic materials.

#### 4. Peridynamic Modeling of Hyperelasticity

In continuum mechanics, the strain energy density for an arbitrary isotropic hyperelastic material corresponds to a function  $\psi(I_1, I_2, I_3)$  where

$$\begin{aligned} I_1 &= \lambda_1^2 + \lambda_2^2 + \lambda_3^2, \\ I_2 &= \lambda_1^4 + \lambda_2^4 + \lambda_3^4, \\ I_3 &= \lambda_1^2 \lambda_2^2 \lambda_3^2. \end{aligned} \quad (11)$$

To make the material easier to control, Xu and colleagues [XSZB15] decouple  $\psi$  into several independent functions involving  $\lambda_1$ ,  $\lambda_2$  and  $\lambda_3$ . Similarly, we define the strain energy density for peridynamic hyperelastic materials as

$$W(\theta, \tau\langle\xi\rangle) = \lambda g(\theta) + \mu \int_{\mathcal{H}_x} w\langle\xi\rangle \mathcal{G}\langle\xi\rangle h(\tau\langle\xi\rangle) dV_\xi, \quad (12)$$

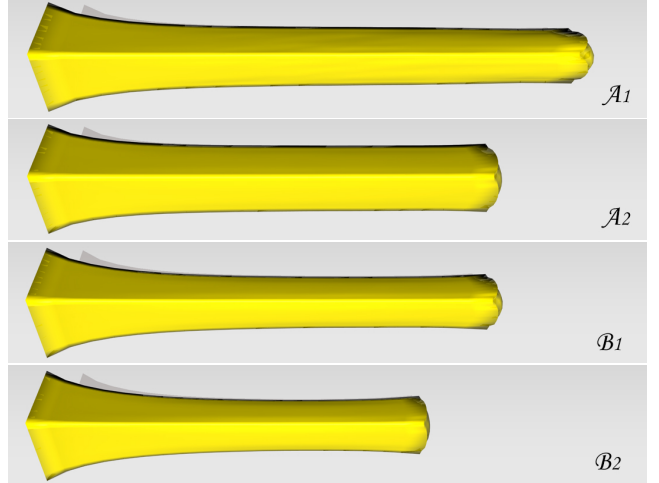


Figure 4: Stretching test. The bar is stretched under a constant tensile force with its material modeled with different basis functions.

where  $g(\theta)$  models the isotropic energy which produces a force similar to the hydrostatic stress in continuum mechanics, while  $h(\tau\langle\xi\rangle)$  models the anisotropic energy.  $w\langle\xi\rangle$  is a normalized weighting function which indicates  $\int_{\mathcal{H}_x} w\langle\xi\rangle dV_\xi = 1$ . The key part that distinguishes our model from a continuum-based method is that we assume the value of  $h(\tau\langle\xi\rangle)$  only depends on the current bond  $\xi$ . Although it is an oversimplification to neglect all other bonds, our model still can create a variety of hyperelastic materials by introducing nonlinear functions  $g$  and  $h$  as well as an anisotropic function  $\mathcal{G}\langle\xi\rangle$  to model the material anisotropy. To design a physical realistic material, nonlinear functions  $g$  and  $h$  should satisfy the following three necessary conditions

- $W(\theta, \tau\langle\xi\rangle) = 0$  at  $\tau\langle\xi\rangle = 1$ ,
- $W(\theta, \tau\langle\xi\rangle)$  reaches its minimum value at  $\tau\langle\xi\rangle = 1$ ,
- $g'' > 0$  and  $h'' > 0$  for all  $\theta, \tau\langle\xi\rangle \in (0, +\infty)$ .

The first condition guarantees there is no stress if no deformation has occurred. The second condition avoids the occurrence of negative strain energy. The third condition ensures that the elastic force will always increase with larger deformation, no matter it is under extension or compression.

By taking the derivative of Equation 12 with respect to  $\mathbf{y}$ , the force vector state for an arbitrary hyperelastic material is written as

$$\begin{aligned} \mathbf{T}(\xi) &= \frac{\partial W(\theta, \tau(\xi))}{\partial \mathbf{y}} \\ &= \frac{w(\xi)}{x(\xi)} (\lambda g'(\theta) + \mu \mathcal{G}(\xi) h'(\tau(\xi))) \frac{\mathbf{y} - \mathbf{y}'}{\|\mathbf{y} - \mathbf{y}'\|} \end{aligned} \quad (13)$$

During the derivation, we redefine  $\theta$  as the following formulation for brevity

$$\theta = \int_{\mathcal{H}_x} w(\xi) \frac{y(\xi)}{x(\xi)} dV_\xi. \quad (14)$$

By invoking the condition  $\int_{\mathcal{H}_x} w(\xi) dV_\xi = 1$ , the value of  $\theta$  calculated from Equation 14 is approximately equal to a third of that calculated from Equation 8. More details on how to calculate  $g'$ ,  $h'$  and  $\mathcal{G}$  will be discussed next.

#### 4.1. Nonlinearity

Since both  $g$  and  $h$  are one-dimensional functions, we can decompose them into a combination of simpler one-dimensional basis functions. In numerical analysis, several kinds of basis functions are available for the decomposition of an arbitrary function  $f(s)$ , among which the most commonly used ones are the Fourier basis and the polynomial basis. Although we can choose any basis function to construct  $W(\theta, \tau(\xi))$ , how to meet the proposed two conditions for the strain energy function is challenging.

According to the concept of a Taylor series, any real stress-strain curve that is infinitely differentiable can be represented as a power series in the form of  $\sum_k a_k s^k$ . However, to inversely construct a physically plausible material, three necessary conditions proposed at Section 4 need to be satisfied. To simplify this process, we prefer to form a set of basis functions with each one satisfying all three necessary conditions. By invoking the strain energy function of typical hyperelastic materials in continuum mechanics, e.g., linear or neo-Hookean materials, we propose to use the following collection to form the basis for  $f(s), s \in (0, +\infty)$

$$\mathcal{A}_n = \frac{1}{n} \left( \frac{s^{n+1} - 1}{n+1} + \frac{s^{-n+1} - 1}{n-1} \right), \mathcal{B}_n = \frac{2}{n} \left( \frac{s^{n+1} - 1}{n+1} - s + 1 \right), \quad (15)$$

where  $n \in \mathbb{Z}^+$  and  $\mathcal{A}_1$  is a special case defined as  $\mathcal{A}_1 = \frac{s^2 - 1}{2} - \log(s)$ . Therefore, the first and second derivatives for each basis can be formulated as follows

$$\mathcal{A}'_n = \frac{s^n - s^{-n}}{n}, \quad \mathcal{B}'_n = \frac{2(s^n - 1)}{n}, \quad (16)$$

$$\mathcal{A}''_n = s^{n-1} + s^{-(n+1)}, \quad \mathcal{B}''_n = 2s^{n-1}. \quad (17)$$

We can also prove that any combination of  $\mathcal{A}_n$  and  $\mathcal{B}_n$  still satisfies all necessary conditions. Figure 3 demonstrates the curves of some basis, it can be noticed that the major difference between  $\mathcal{A}_n$  and  $\mathcal{B}_n$  is that the value of  $\mathcal{A}_n$  reaches  $+\infty$  as  $s$  approaches 0. This has the advantage of providing sufficient repulsive forces as the material is under compression. Figure 5 shows a comparison of the elastic behaviors after applying different basis for modeling elastic materials. When the Armadillo is fallen on the floor, the right example, which we set  $g = \mathcal{A}_4$  and  $h = \mathcal{A}_4$ , can effectively avoid

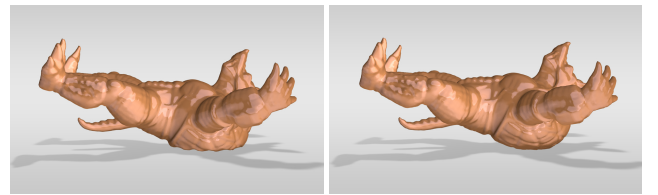


**Figure 5:** Armadillo falling onto the ground. Left: a linear elastic model; Right: a nonlinear elastic model. The nonlinear model produces rich small-deformation dynamics for hands and legs while still gets a plausible simulation at its back.

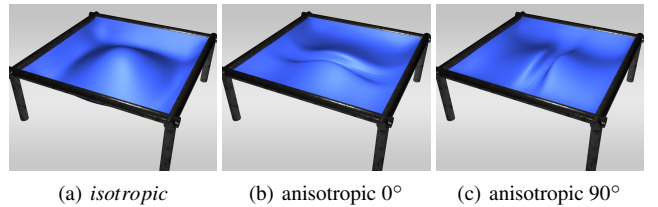


**Figure 6:** A trampoline. Different deformation patterns can be noticed by using isotropic and different anisotropic scalar state. (a) isotropic, (b) (c) anisotropic with different rotation matrixes.

unnatural behaviors for regions under compression compared to the left example, which we only adopted a linear elastic model by setting  $g = \mathcal{B}_1$  and  $h = \mathcal{B}_1$ .

#### 4.2. Anisotropy

Although it is possible to design an anisotropic function to model the material anisotropy, we prefer not to do so in our practical implementation due to the complexity of designing a function that is both anisotropic and nonlinear. Instead, we introduce an anisotropic scalar state  $\mathcal{G}(\xi)$  to control the material anisotropy independently, which greatly simplifies the designing of anisotropic materials. Inspired by the orthotropic material proposed by Xu and colleagues [XSZB15], our anisotropic scalar state can be characterized with its three orthotropic material directions and their respective intensity.

$$\mathcal{G}(\xi) = \left\| \Sigma \mathbf{R} \frac{\mathbf{x}' - \mathbf{x}}{\|\mathbf{x}' - \mathbf{x}\|} \right\|, \quad (18)$$

where  $\mathbf{R}$  is a rotation matrix with its three column vectors representing three orthotropic material directions.  $\Sigma$  is a diagonal matrix with three diagonals  $\sigma_1, \sigma_2, \sigma_3$  to control the force magnitude in each material direction. Besides, we require the condition  $\sigma_1 \sigma_2 \sigma_3 = 1$  should always be satisfied to ensure that  $\mathcal{G}$  only contributes to model the material anisotropy without affecting the overall material stiffness. Figure 6 shows an example simulated with different material anisotropy. The three diagonal elements of  $\Sigma$  are initially set to  $\sigma_1 = 4, \sigma_2 = 0.25$  and  $\sigma_3 = 1.0$ .

## 5. Numerical Solution

In this section, we will describe how to apply a quasi-Newton method to solve the dynamics of a hyperelastic material.

### 5.1. Discretization

In our implementation, the peridynamic body is discretized into individual particles with each particle  $i$  carrying the reference position  $\mathbf{x}_i$ , current position  $\mathbf{y}_i$ , mass  $m_i$ , and volume  $V_i$ , etc. According to Equation 13, the elastic force imposed on particle  $i$  by its neighboring particle  $j$  is written as

$$\mathbf{T}_{ij} = \frac{w_{ij}}{x_{ij}} (\lambda g'(\theta_i) + \mu G_{ij} h'(\tau_{ij})) \frac{\mathbf{y}_j - \mathbf{y}_i}{|\mathbf{y}_j - \mathbf{y}_i|}, \sum_{j \in \mathcal{H}_i} w_{ij} V_j = 1 \quad (19)$$

where the subscript  $ij$  represents the bond  $\xi = \mathbf{x}_i - \mathbf{x}_j$  and  $\theta_i$  is calculated from Equation 14 with particle discretization. The governing equations for each particle  $i$  can then be formulated as

$$m_i \ddot{\mathbf{u}}_i = V_i \sum_{j \in \mathcal{H}_i} (\mathbf{T}_{ij} - \mathbf{T}_{ji}) V_j + \mathbf{f}_i^{ext} \quad (20)$$

where  $\mathbf{f}_i^{ext} = \mathbf{b}_i V_i$ . An easy approach to solve Equation 20 is by applying an explicit Euler method. However, its stability depends on the choice of the timestep size. Therefore, we seek to implement an implicit method to improve the simulation stability. From the view point of energy, Equation 20 is equivalent to solving the following energy minimization problem

$$E(\mathbf{q}) = \min_{\mathbf{q}^{n+1}} \left( \frac{\mathbf{M}}{2\Delta t^2} \|\mathbf{q}^{n+1} - \mathbf{q}^*\|^2 + \sum_i W(\theta_i, \tau_{ij}) V_i \right) \quad (21)$$

where  $\mathbf{M}$  is the mass-matrix,  $\Delta t$  is the simulation step size,  $\mathbf{q}$  is a vector with all particles' current positions assembled together and  $\mathbf{q}^*$  is an intermediate state with  $\mathbf{q}^* = \mathbf{q}^n + \Delta t \mathbf{v}^n + \Delta t^2 \mathbf{M}^{-1} \mathbf{f}^{ext}$ . Note that  $W(\theta_i, \tau_{ij})$  represents a function of the dilatation  $\theta_i$  and all independent bond stretches  $\tau_{ij}$ . By reapplying the Newton method, the energy minimization problem can be solved iteratively with the following equation

$$(\mathbf{K} + \frac{\mathbf{M}}{\Delta t^2})(\mathbf{q}^{k+1} - \mathbf{q}^k) = \frac{\mathbf{M}}{\Delta t^2}(\mathbf{q}^* - \mathbf{q}^k) + \nabla_{\mathbf{q}^k} \sum_i W(\theta_i, \tau_{ij}) V_i \quad (22)$$

where  $\mathbf{q}^k$  represents the solution of  $k$ -th iteration,  $\mathbf{K}$  is the stiffness matrix which can be calculated as the second derivative of the total strain energy, and  $\nabla_{\mathbf{q}^k}$  represents a gradient operator with respect to  $\mathbf{q}^k$ . By taking enough iterations,  $\mathbf{q}^{k+1}$  will finally converge to the exact solution. However, since the value of  $\mathbf{K}$  varies at each iteration, it can be very time-consuming if we directly use the Newton method to solve the governing equations for hyperelastic materials.

### 5.2. Quasi-Newton Method

We implement the quasi-Newton method proposed by Liu and his colleagues [LBBK17]. The key idea is to replace the exact Hessian matrix  $\mathbf{K}$  with an approximate one defined as follows

$$\mathbf{L} = \left( \sum_i \sum_{j \in \mathcal{H}_i} k_{ij} \mathbf{A}_{ij} \mathbf{A}_{ij}^T \right) \otimes I_3 \quad (23)$$

with  $k_{ij}$  represents the stiffness for each bond in the reference configuration, defined as  $k_{ij} = \frac{w_{ij}}{x_{ij}^2} (\lambda g''(1) + \mu G_{ij} h''(1))$ .  $\mathbf{A}_{ij}$  is a column vector of dimension  $n$  (number of all discrete points),  $\mathbf{A}_{ij,i} = 1, \mathbf{A}_{ij,j} = -1, \mathbf{A}_{ij,other} = 0$ .  $\otimes$  is the kronecker product. Due to above approximation, the Hessian matrix can be pre-computed at the beginning of simulation to accelerate solving the linear system

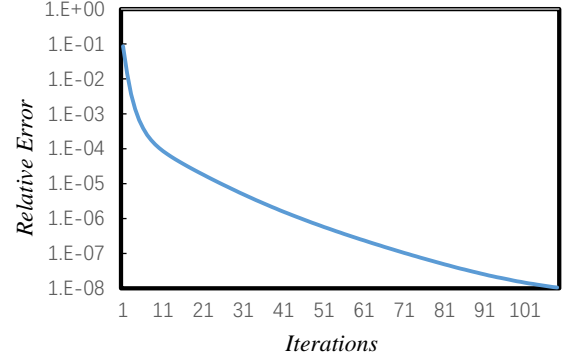


**Figure 7:** The decrease of the relative error with respect to the iteration count for the turtle example at time  $t = 0.8s$ .

Name	freedom	$\Delta t$ (s)	iters	$t_f$ (ms)
Flower	5.4K	0.04	20.3	104
Armadillo	18K	0.01	9.6	323
Wrinkle Cloth	10.8K	0.01	6.2	146
Cylinder	2.5K	0.04	10.4	57
Bunny	35K	0.01	16.8	1300

**Table 1:** Statistics and timings of our examples,  $t_f$  is the average time per frame.

of equations. However, one side effect is that we still need to take an extra line search strategy to find a local minimum.

**Line Search** The line search is taken as follows. At the end of each iteration  $k$ , we check the value of  $E(\mathbf{q}^{k+1})$  and compare it to  $E(\mathbf{q}^k)$ . If  $E(\mathbf{q}^{k+1})$  is smaller, we accept  $\mathbf{q}^{k+1}$  as the solution of iteration  $k$ . Otherwise, we need to further check the value of  $E(\mathbf{q}^*)$  where  $\mathbf{q}^*$  is the middle point of  $\mathbf{q}^{k+1}$  and  $\mathbf{q}^k$ . We repeat this until we find a point that decreases the total energy.

### 6. Results and Discussions

In our implementation, we solve the linear system of equations on a CPU (Intel Core i5-7500 3.4GHz) while calculate other parts in parallel on a GPU (GTX 1060 3G). In case an object is experiencing an extreme deformation under large external forces, it is hard for our current model to prevent shape inversion. To see this, consider an undeformed object whose shape is suddenly inverted, the total strain energy will still remain zero, therefore no force will help recover the object to its initial state. Motivated by He and his colleagues's recent work [HWW17], we propose to add the following force to prevent shape inversion

$$\mathbf{T}_{ij}^{inv} = k_{ij} [\mathbf{y}_i - \mathbf{y}_j - \bar{\mathbf{F}}_i(\mathbf{x}_i - \mathbf{x}_j)] \quad (24)$$

where  $\bar{\mathbf{F}}_i$  is the particle approximation of the deformation gradient calculated from particle  $i$ 's neighborhood. In case shape inversion occurs for particle  $i$ , i.e.,  $|\bar{\mathbf{F}}_i| < 0$ , we only need to exchange the first two rows of  $\bar{\mathbf{F}}_i$  to help recover the shape.

**Convergence Analysis.** We evaluate the convergence of our

method with the relative error, defined as

$$\frac{E(\mathbf{q}^k) - E(\mathbf{q})}{E(\mathbf{q}^0) - E(\mathbf{q})} \quad (25)$$

redwhere  $\mathbf{q}^0$  is the initial guess and  $\mathbf{q}^k$  is the solution at  $k - th$  iteration. Figure 7 plots the convergence rate at a chosen time for the turtle example, where  $\mathbf{q}$  represents the final solution when  $E(\mathbf{q}^k) - E(\mathbf{q}^{k+1})$  is smaller than our predefined threshold  $(1/2)^{10}$ . In this test, a minimum relative error of  $1 \times 10^{-8}$  is reached. However, in our practical implementation, we typically use  $\mathbf{q}^{k+1}$  instead of the final solution for saving time. We find a relative error of  $1 \times 10^{-4}$  would be enough for most examples. Therefore,  $5 \sim 25$  iterations will be enough. Table 1 presents the statistics and timings of our examples.

**Poisson's ratio.** According to the definition of the strain energy density in Equation 12, there are two parameters that characterize the elastic behaviors of hyperelastic materials for selected basis functions. Although it is possible to relate  $\lambda$  and  $\mu$  to physical parameters in continuum mechanics for small deformations, as was done in [SA05], strictly setting up their equivalence for any large deformations is not possible. redTherefore, by equating the total strain energies of our model with a classical linear elastic model, we provide the following approximate relationship to help readers familiar with continuum mechanics model hyperelastic materials more easily

$$\lambda = \frac{9E_Y v}{2(1+v)(1-2v)}, \quad \mu = \frac{15E_Y}{4(1+v)}. \quad (26)$$

$E_Y$  and  $v$  represents Young's modulus and Poisson's ratio, respectively. By setting  $v$  to different values, Figure 8 demonstrates how our method can effectively generate materials with different Poisson's ratios. For this example, we set Young's modulus to  $1 \times 10^5$  for all three examples and use  $\mathcal{B}_1$  as the basis function.

**Bending.** Theoretically speaking, the bending effect of a cloth should be controlled by its thickness. However, for a cloth represented with only one layer of particles, it is feasible within our model to control the cloth bending by adjusting the radius of  $\mathcal{H}$ . In other words, a larger radius for  $\mathcal{H}$  indicates more neighboring particles can take part in resisting the bending of a cloth. By choosing different weighting functions and radii of  $\mathcal{H}$ , Figure 9 demonstrates a comparison where the left example is taken with  $\delta = 2d$ ,  $w(\xi) = (1 + \frac{|\xi|}{\delta})^{-1}$  and the right one with  $\delta = 4d$ ,  $w(\xi) = \frac{|\xi|}{\delta}$ . We can notice that a larger bending resistance for a larger radius of  $\mathcal{H}$ .

**Twisting.** Figure 10 demonstrates an example to show how our method can robustly simulate the twisting of a bar. During the simulation, we rotate a total of 360 degrees for the left end of the bar while keep the right end fixed.

**Collision.** Figure 11 shows an collision example of several objects assigned with different materials. The materials for the armadillo, ball, bunny, cloth and teapot are set to be linear, linear, nonlinear, anisotropic linear and anisotropic nonlinear, respectively. All objects except the cloth retain the same Young's modulus ( $E_Y = 5.0 \times 10^5$ ) and Poisson's ratio ( $v = 0.25$ ). The Young's modulus of the cloth is set to  $1.0 \times 10^4$ . Collisions between objects are handled with the position-based method [BMM15].

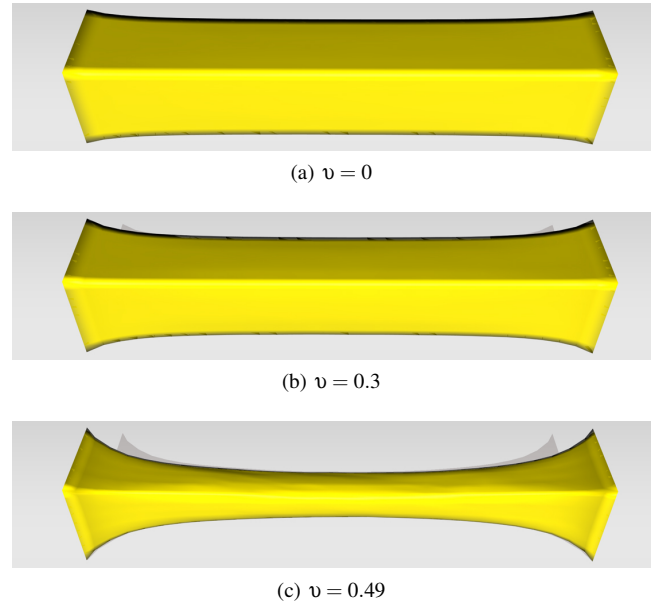


**Figure 8:** Bar stretching. Our method can simulate different elastic behaviors with different Poisson's ratios and use different weighting functions.

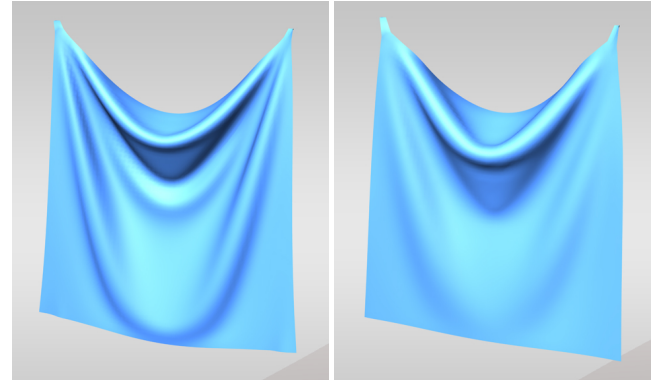


**Figure 9:** The cloth example. Our method can simulate different bending stiffness behaviors by adjusting the radius of  $\mathcal{H}$ .

**Neo-Hookean Material.** To approximately model a neo-Hookean material, which is defined as

$$\Psi(I_1, J) = \frac{\bar{\mu}}{2}(I_1 - 3) - \bar{\mu}\log(J) + \frac{\bar{\lambda}}{2}\log^2(J) \quad (27)$$

in continuum mechanics, where  $\bar{\lambda}$  and  $\bar{\mu}$  represent the Lamé constants, we consider an uniaxial deformation along the  $x$  direction whose deformation gradient is  $\mathbf{F} = diag(s, 1, 1)$ . The strain energy density can then be reformulated as  $\bar{\mu}(\frac{s^2-1}{2} - \log(s)) + \frac{\bar{\lambda}}{2}(\log^2(s))$ . The most appropriate basis functions should be  $h(s) = \mathcal{A}_1$  and  $g(s) = \log^2(s)$ . However, since  $\log^2(s)$  does not belong to any of our basis functions, we simply set  $g(s) = h(s) = \mathcal{A}_1$ . redFigure 12 demonstrates the stress-strain curves of a linear and neo-Hookean elastic bar in tension. We can note the results are comparable to those generated by FEM with our current choice of the basis func-

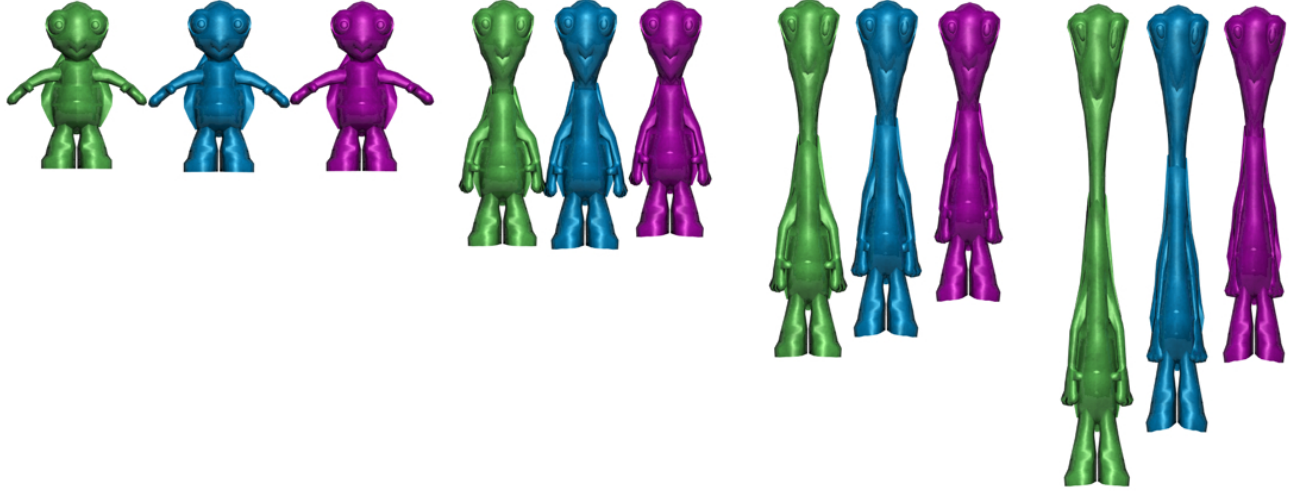


**Figure 13:** Green is a neo-Hookean material. Blue is our approximation for a neo-Hookean in peridynamics. Purple is a linear peridynamics solid. All three turtles are simulated with the same Young's modulus and Poisson's ratio. From left to right is deformation under 0.1x, 1x, 2x, 3x gravity.

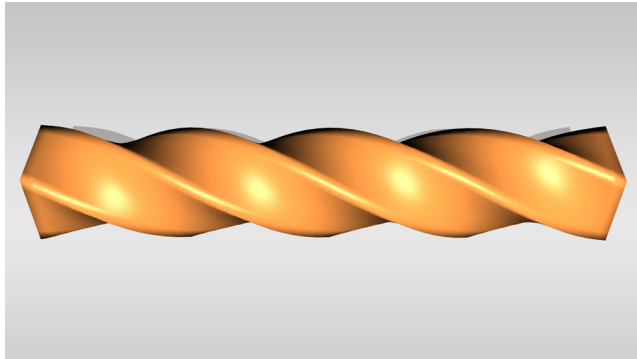


**Figure 10:** Bar twisting. The left end of a bar is rotated 360 degrees to test the stability of our method.

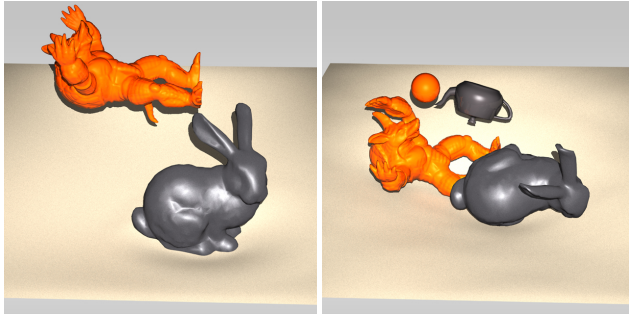


**Figure 11:** Deformable objects falling onto a soft cloth. The materials for armadillo, ball, bunny, cloth and teapot are set to be linear, linear; nonlinear, anisotropic linear and anisotropic nonlinear, respectively.

tions. However, to exactly match the simulation results, we should choose the right basis functions with more care. Figure 13 further

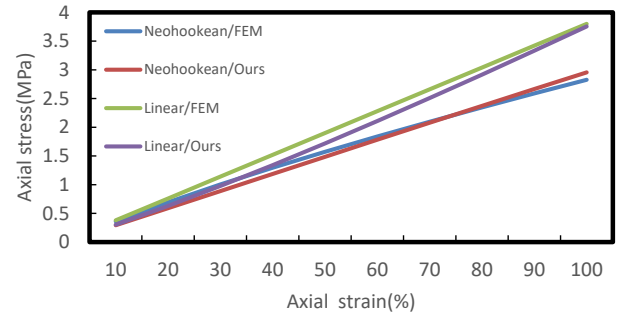


**Figure 12:** Stress-strain curves for various elastic material models.

evaluated the accuracy of our model by simulating an elastic turtle.

**StVK Material.** The strain-energy density function for the St. Venant-Kirchhoff model in continuum mechanics is

$$\Psi(\mathbf{F}) = \bar{\mu} \mathbf{E} : \mathbf{E} + \frac{\bar{\lambda}}{2} \text{tr}^2(\mathbf{E}), \quad (28)$$

Similarly, for the above uniaxial deformation, the strain energy can be reformulated as  $\bar{\mu} \left( \frac{s^2 - 1}{2} \right)^2 + \frac{\bar{\lambda}}{2} \left( \frac{s^2 - 1}{2} \right)^2$ , we therefore set  $g(s) = h(s) = \left( \frac{s^2 - 1}{2} \right)^2 = \frac{3B_3 - B_1}{2}$ . Figure 14 presents a comparison between our model and FEM in simulating a deformable Stanford bunny. We can notice similar simulation results for both methods. However, experiments show that our model has a better stability in simulating large deformations compared to the finite element method. It can be noticed from the video that simulation with FEM breaks down after being imposed with a large external force while our method remains stable during the whole simulation.

**Flower.** In Figure 1, we present an interesting example by exerting several different external forces to a flower model. The flower is treated as a nonlinear and heterogenous StVK material.

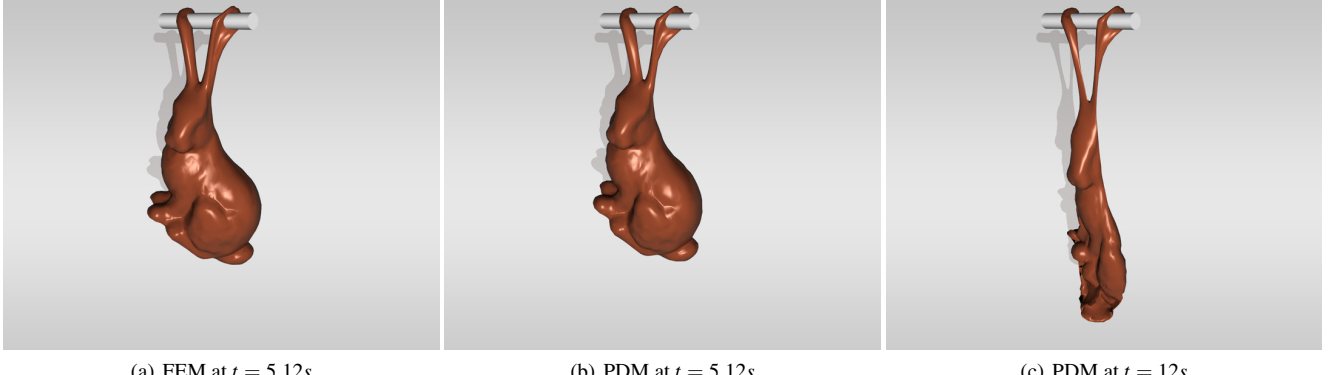


**Figure 14:** The bunny example. Our method is robust at simulating the StVK material while FEM breaks down at large deformations, both of which are simulated with the same Young’s modulus and Poisson’s ratio.

**Limitations.** The major limitation of our method is that our method requires a manual selection of the basis functions to construct redan appropriate strain energy function for a given hyperelastic material. Besides, some degree of parameter tuning is also necessary in order to match the simulation result to a given deformation sequence. However, since artificial neural network has been widely used in a lot of areas as well as in material modeling [JG06, UK09, CT17], we believe integrating neural networks into our method can greatly alleviate above mentioned problems.

## 7. Conclusion

In this paper, we present a general strain energy model for peridynamics to simulate various hyperelastic materials involving non-linearity and anisotropy. The new model is intuitive, flexible and easy to implement. But just like other continuum-based hyperelastic models, our peridynamic-based hyperelastic model still only constitutes a subspace of all nonlinear isotropic and anisotropic materials. Besides, the theoretical equivalence to the classical elastic theory is also unclear.

Since peridynamics is still an on-going research area, much efforts need to be done to improve both its fundamental theory and numerical solvers. For our future work, we will first explore whether we can equal peridynamics to the classical elastic theory for certain hyperelastic models. To improve the simulation performance, we would also like to explore more efficient implicit solver for real-time applications. Finally, since peridynamics was initially invented for simulating fracture, which is also demonstrated in the video with a cloth tearing example by integrating the bond failure condition [SA05] into an anisotropic elastic model, it would be interesting to know whether we can use neural networks to design the desired hyperelastic materials and various fracture patterns.

## 8. Acknowledgement

We would like to thank anonymous reviewers for their valuable comments, Kuixin Zhu and Congyi Zhang for modeling and rendering. The project was supported by the National Key R&D Program of China (No.2017YFB1002700, No.2017YFB0203002),

the National Natural Science Foundation of China (No.61472010, No.6187070657, No.61661146002), Key Research Program of Frontier Sciences, CAS (No. QYZDY-SSW-JSC041).

## References

- [BBO<sup>\*</sup>09] BICKEL B., BÄCHER M., OTADUY M. A., MATUSIK W., PFISTER H., GROSS M.: Capture and modeling of non-linear heterogeneous soft tissue. *ACM Transactions on Graphics (TOG)* 28, 3 (2009), 89. 2
- [BC00] BOURGUIGNON D., CANI M.-P.: Controlling anisotropy in mass-spring systems. In *Computer animation and simulation* (2000), vol. 2000, Springer, pp. 113–123. 2
- [BIT09] BECKER M., IHMSEN M., TESCHNER M.: Corotated SPH for deformable solids. In *Eurographics Workshop on Natural Phenomena* (2009), Citeseer, pp. 27–34. 2
- [BJ05] BARBIĆ J., JAMES D. L.: Real-time subspace integration for st. venant-kirchhoff deformable models. 982–990. 2
- [BML<sup>\*</sup>14] BOUAZIZ S., MARTIN S., LIU T., KAVAN L., PAULY M.: Projective dynamics: Fusing constraint projections for fast simulation. *ACM Trans. Graph. (SIGGRAPH)* 33, 4 (2014), 154:1–154:11. 2
- [BMM15] BENDER J., MÜLLER M., MACKLIN M.: Position-based simulation methods in computer graphics. *EUROGRAPHICS Tutorial Notes* (2015). 7
- [CLSM15] CHEN D., LEVIN D. I., SUEDA S., MATUSIK W.: Data-driven finite elements for geometry and material design. *ACM Transactions on Graphics (TOG)* 34, 4 (2015), 74. 2
- [CT17] CHU M., THUEREY N.: Data-driven synthesis of smoke flows with cnn-based feature descriptors. *arXiv preprint arXiv:1705.01425* (2017). 9
- [CZZ<sup>\*</sup>17] CHEN W., ZHU F., ZHAO J., LI S., WANG G.: Peridynamics-based fracture animation for elastoplastic solids. *Computer Graphics Forum* 37, 1 (2017), 112–124. 3
- [DG96] DESBRUN M., GASCUEL M.-P.: *Smoothed particles: A new paradigm for animating highly deformable bodies*. Springer, 1996. 2
- [GHF<sup>\*</sup>07] GOLDENTHAL R., HARMON D., FATTAL R., BERCOVIER M., GRINSPUN E.: Efficient simulation of inextensible cloth. *ACM Trans. Graph.* 26, 3 (July 2007). 2
- [GM97] GIBSON S. F., MIRTICH B.: *A survey of deformable modeling in computer graphics*. Tech. rep., Technical Report, Mitsubishi Electric Research Laboratories, 1997. 2
- [GSS07] GERSTLE W., SAU N., SILLING S.: Peridynamic modeling of concrete structures. *Nuclear engineering and design* 237, 12-13 (2007), 1250–1258. 1

- [HHBS12] HU W., HA Y. D., BOBARU F., SILLING S. A.: The formulation and computation of the nonlocal j-integral in bond-based peridynamics. *International journal of fracture* 176, 2 (2012), 195–206. [1](#)
- [HWW17] HE X., WANG H., WU E.: Projective peridynamics for modeling versatile elastoplastic materials. *IEEE transactions on visualization and computer graphics* (2017). [2](#), [3](#), [6](#)
- [JG06] JUNG S., GHABOSSI J.: Neural network constitutive model for rate-dependent materials. *Computers & Structures* 84, 15 (2006), 955–963. [9](#)
- [JWJ\*14] JONES B., WARD S., JALLEPALLI A., PERENIA J., BARGTEIL A. W.: Deformation embedding for point-based elastoplastic simulation. *ACM Trans. Graph.* 33, 2 (2014), 21. [2](#)
- [KMOD09] KHAREVYCH L., MULLEN P., OWHADI H., DESBRUN M.: Numerical coarsening of inhomogeneous elastic materials. *ACM Transactions on Graphics (TOG)* 28, 3 (2009), 51. [2](#)
- [LB14] LI Y., BARBIĆ J.: Stable orthotropic materials. In *Proceedings of the ACM SIGGRAPH/Eurographics Symposium on Computer Animation* (2014), Eurographics Association, pp. 41–46. [2](#)
- [LB15] LI Y., BARBIĆ J.: Stable anisotropic materials. *IEEE transactions on visualization and computer graphics* 21, 10 (2015), 1129–1137. [2](#)
- [LBC\*14] LEVINE J. A., BARGTEIL A. W., CORSI C., TESSENDORF J., GEIST R.: A peridynamic perspective on spring-mass fracture. In *Proceedings of the ACM SIGGRAPH/Eurographics Symposium on Computer Animation* (2014), Eurographics Association, pp. 47–55. [2](#), [3](#)
- [LBK17] LIU T., BOUAZIZ S., KAVAN L.: Quasi-newton methods for real-time simulation of hyperelastic materials. *ACM Trans. Graph.* 36 (2017). [2](#), [6](#)
- [LBOK13] LIU T., BARGTEIL A. W., O'BRIEN J. F., KAVAN L.: Fast simulation of mass-spring systems. *ACM Trans. Graph. (SIGGRAPH Asia)* 32, 6 (Nov. 2013), 214:1–214:7. [2](#)
- [MC11] MÜLLER M., CHENTANEZ N.: Solid simulation with oriented particles. *ACM Trans. Graph.* 30, 4 (July 2011), 92:1–92:10. [2](#)
- [MG04] MÜLLER M., GROSS M.: Interactive virtual materials. In *Proceedings of Graphics Interface 2004* (2004), Canadian Human-Computer Communications Society, pp. 239–246. [2](#)
- [MHHR07] MÜLLER M., HEIDELBERGER B., HENNIX M., RATCLIFF J.: Position based dynamics. *J. Vis. Comun. Image Represent.* 18, 2 (Apr. 2007), 109–118. [2](#)
- [MMCK14] MACKLIN M., MÜLLER M., CHENTANEZ N., KIM T.-Y.: Unified particle physics for real-time applications. *ACM Trans. Graph. (SIGGRAPH)* 33, 4 (2014), 153. [2](#)
- [MZS\*11] MCADAMS A., ZHU Y., SELLE A., EMPEY M., TAMSTORF R., TERAN J., SIFAKIS E.: Efficient elasticity for character skinning with contact and collisions. In *ACM Transactions on Graphics (TOG)* (2011), vol. 30, ACM, p. 37. [2](#)
- [NOB16] NARAIN R., OVERBY M., BROWN G. E.: Admm  $\supseteq$  projective dynamics: fast simulation of general constitutive models. In *Symposium on Computer Animation* (2016), pp. 21–28. [2](#)
- [OH99] O'BRIEN J. F., HODGINS J. K.: Graphical modeling and animation of brittle fracture. In *Proceedings of the 26th annual conference on Computer graphics and interactive techniques* (1999), ACM Press/Addison-Wesley Publishing Co., pp. 137–146. [2](#)
- [PDA01] PICINBONO G., DELINGETTE H., AYACHE N.: Nonlinear and anisotropic elastic soft tissue models for medical simulation. In *Robotics and Automation, 2001. Proceedings 2001 ICRA. IEEE International Conference on* (2001), vol. 2, IEEE, pp. 1370–1375. [2](#)
- [RJ07] RIVERS A. R., JAMES D. L.: Fastlsm: fast lattice shape matching for robust real-time deformation. 82. [2](#)
- [SA05] SILLING S. A., ASKARI E.: A meshfree method based on the peridynamic model of solid mechanics. *Computers & structures* 83, 17–18 (2005), 1526–1535. [7](#), [9](#)
- [SB05] SILLING S. A., BOBARU F.: Peridynamic modeling of membranes and fibers. *International Journal of Non-Linear Mechanics* 40, 2-3 (2005), 395–409. [1](#)
- [SEW\*07] SILLING S. A., EPTON M., WECKNER O., XU J., ASKARI E.: Peridynamic states and constitutive modeling. *Journal of Elasticity* 88, 2 (2007), 151–184. [3](#)
- [Sil00] SILLING S. A.: Reformulation of elasticity theory for discontinuities and long-range forces. *Journal of the Mechanics and Physics of Solids* 48, 1 (2000), 175–209. [1](#), [3](#)
- [SL08] SILLING S. A., LEHOUCQ R. B.: Convergence of peridynamics to classical elasticity theory. *Journal of Elasticity* 93, 1 (2008), 13. [1](#)
- [STC\*12] SCHUMACHER C., THOMASZEWSKI B., COROS S., MARTIN S., SUMNER R., GROSS M.: Efficient simulation of example-based materials. In *Proceedings of the ACM SIGGRAPH/eurographics symposium on computer animation* (2012), Eurographics Association, pp. 1–8. [2](#)
- [UK09] UNGER J. F., KÖNKE C.: Neural networks as material models within a multiscale approach. *Computers & Structures* 87, 19 (2009), 1177–1186. [9](#)
- [VMTF09] VOLINO P., MAGNENAT-THALMANN N., FAURE F.: A simple approach to nonlinear tensile stiffness for accurate cloth simulation. *ACM Transactions on Graphics* 28, 4 (2009), Article No. 2
- [WDGT01] WU X., DOWNES M. S., GOKTEKIN T., TENDICK F.: Adaptive nonlinear finite elements for deformable body simulation using dynamic progressive meshes. In *Computer Graphics Forum* (2001), vol. 20, Wiley Online Library, pp. 349–358. [2](#)
- [WY16] WANG H., YANG Y.: Descent methods for elastic body simulation on the gpu. *ACM Transactions on Graphics (TOG)* 35, 6 (2016), 212. [2](#)
- [XSZB15] XU H., SIN F., ZHU Y., BARBIĆ J.: Nonlinear material design using principal stretches. *ACM Transactions on Graphics (TOG)* 34, 4 (2015), 75. [2](#), [4](#), [5](#)